ORIGINAL ARTICLE

Investigation of Microstructure and Mechanical Properties of DSS 2205 Weld Thick Section for Pressure Vessel Application

Sagarkumar I. Shah[1,2] · Hemantkumar R. Thakkar[3] · Kiritkumar Patel[4] · G. D. Acharya[2]

Abstract Number of Industries including marine, oil and gas, pharmaceutical are facing challenges in welding of thick section duplex stainless steel (DSS) to attain desired microstructure and mechanical properties. The DSS is dual phase structure comprising of austenite and ferrite in equal proportion. The present work is aimed to investigate microstructure and mechanical properties of DSS 2205 thick (20 mm) plate weld for pressure vessel by multi-pass shielded metal arc welding using E2209 electrode to maintain heat input 0.5–1.5 kJ/mm. Weldment was tested for ferrite measurement, tensile, impact, hardness and bend test by cutting across the weld. Scanning electron microscope and optical microscope were used to examine microstructures at weld zone and heat affected zone. In microscopic examination, widmanstetten austenite, intra granular austenite and grain boundary austenite were observed in weld zone while partially transformed austenite in heat affected zone.

Keywords DSS 2205—duplex stainless steel · SMAW—shielded metal arc welding · Mechanical properties · Microstructure · Pressure vessel

✉ Sagarkumar I. Shah
  shahsagar.7@gmail.com

1 Gujarat Technological University, Ahmedabad, Gujarat, India

2 Atmiya Institute of Technology and Science, Rajkot, Gujarat, India

3 Mechanical Enginnering Department, G. H. Patel College of Engineering and Technology, V.V.Nagar, Anand, Gujarat, India

4 GMM Pfaudler, V.V.Nagar, Anand, Gujarat, India

1 Introduction

Duplex stainless steels (DSSs) are Cr–Ni–Fe-based alloys and combination of dual structure of austenite (γ) and ferrite (δ) in equal proportion [1–3]. DSS is one of the better options for a good corrosion resistance and mechanical properties in various aggressive environments like chemical, marine, petrochemical, pharmaceutical and heavy engineering applications [4–7]. However, it is a severe issue to maintain austenite-ferrite ratio 50:50 in various conditions like heat treatment, welding and high temperature to attain excellent properties in DSS [8–10]. DSS exhibits good weldability compared to Austenitic Stainless Steel (ASS) but due to cooling rate, electrode chemistry and energy density, austenite-ferrite ratio can get altered in weld/fusion zone (WZ/FZ) and heat affected zone (HAZ) during welding process [11]. The ill effect of very high peak temperature which is more than temperature of ferrite solvus is that, ferrite distribution in heat affected and fusion zone becomes high. This may lead to fusion/weld zone possessing ferrite content more than 50% and to overcome this issue filler material is added with higher austenite stabilizers than base metal for balancing austenite-ferrite ratio [12].

The heat input also play a crucial role in DSS welding to balance austenite-ferrite ratio. Normally, slow cooling rate is more preferable to maintain fraction of austenite-ferrite which is possibly attained at higher heat input with wide HAZ and large grain size in FZ. On the other side, adverse effect of high heat input leads to intermetallic phase formation such as σ, χ chromium nitride and other phases during DSS welding [13–18]. Mechanism of precipitation and transformation involves depletion of corrosion resistant elements in the region contiguous to the precipitates near the secondary austenite zone of the austenite-ferrite

Table 1 DSS 2205 chemical composition in % wt

Element	C	P	Mn	Si	S	Ni	Cr	N	Mo
% wt	0.019	0.024	1.138	0.565	0.006	8.456	23.363	0.2168	3.285

Table 2 E 2209 chemical composition in % wt

Element	C	P	Mn	Si	S	Cr	Ni	Mo	N
% wt	0.004	0.030	1.0	0.5	0.025	23.0	9.0	3.0	0.15

interface [19–23]. This adversely influences the susceptibility of DSSs to intergranular corrosion (IGC).

Sensitization occurs in DSSs which leads to intermetallic phase formation and deterioration of mechanical properties accordingly revealed by many researchers in the case of isothermal heating [24–27]. To prevent intermetallic precipitations like as σ, χ chromium nitride, etc. and maintain austenite-ferrite ratio during DSS welding, sufficient cooling is required after welding is necessary [28]. Shielded metal arc welding (SMAW) is majorly preferred due to its flexibility, portability and simplicity [1, 2]. Schaeffler and Delong diagram WRC-1992 is important to predict weld metal microstructure based on chromium-nickel equivalent. In actual practice, these diagrams are less preferred because it is not considering effect of cooling rate during welding [29–31]. Imbalance in microstructure also reveals that corrosion behavior is different for base metal, heat affected zone and weld zone [1].

Secondary phases easily precipitate as dual phase of austenite/ferrite interface than that of single phase of austenite or ferrite [4]. However, extensive investigation has been carried out on DSSs in context of microstructures and mechanical properties for thin sections, but very less information is reported on the influence of intermetallic phase on microstructural changes and mechanical properties in thick section of DSS weld. This research intends to investigate the mechanical properties and microstructural

changes in 20-mm-thick section by multipass SMAW for pressure vessel.

2 Experimental Work

2.1 Materials

In this research, commercial grade of duplex stainless steel DSS 2205 has been used for experimental work. The test coupons were taken from welded DSS 2205 plate having size of 300 mm length, 270 mm wide and 20 mm thickness. Chemical analysis of DSS 2205 was done as per ASTM E 1086:14 [32] using Shimadzu PDA-7000, and Table 1 shows average chemical composition percentage weight.

2.2 Welding Procedure

DSS 2205 was manually welded by shielded metal arc welding (SMAW) using WARPP INTIG-400 I machine. E 2209–15 was used as welding consumable and average chemical analysis in percentage weight is given in Table 2. Welding consumable was heated at 300 °C for 2 h in oven for excellent weldability. For SMAW, joint was prepared by single V butt joint having root gap of 2 mm and root face of 1.5 mm. Complete welding was carried out by total 20 passes from which 3 passes were used for back

Table 3 Welding parameters for SMAW

Pass	Volt (V)	Amperage (A)	Travel speed (mm/min)	Heat input (kJ/mm)	Interpass temperature (°C)
Root	22–28	85–90	117	1.29	–
Filler	18–32	139–142	190–235	1.19–1.35	150
Cap	19–33	140–142	265–290	0.95–1.02	150

Table 4 Ferrite % of various zones

Location	Avg. % Ferrite
WZ	43.526
HAZ	48.219
BM	50.788

chipping. During welding, interpass temperature was maintained to 150 °C using infrared thermometer HTC MT-4 between two consecutive passes. The welding parameters for SMAW are given in Table 3. Welded specimen was also tested for radiography test as per ASME Sec. V [33].

2.3 Ferrite Measurement and Microstructure Analysis

Welded specimen was analyzed for ferrite content at base metal, weld zone and heat affected zone using calibrated Helmut Fischer GMBH FMP30 to evaluate ferrite volume fraction. Each value of ferrite measurement was taken by calculating average of five observations. Then samples were prepared as per ASTM E3—95 [34] for scanning electron microscope (SEM), energy dispersive spectroscopy (EDS) to investigate microstructural changes during welding. Optical microscopic examination was analyzed using optical microscope NIM1000X and SEM as well as EDS was carried out using JEOL (JSM5610LV). Intermetallic phase analysis was also carried out for WZ and HAZ as per ASTM A923 [35].
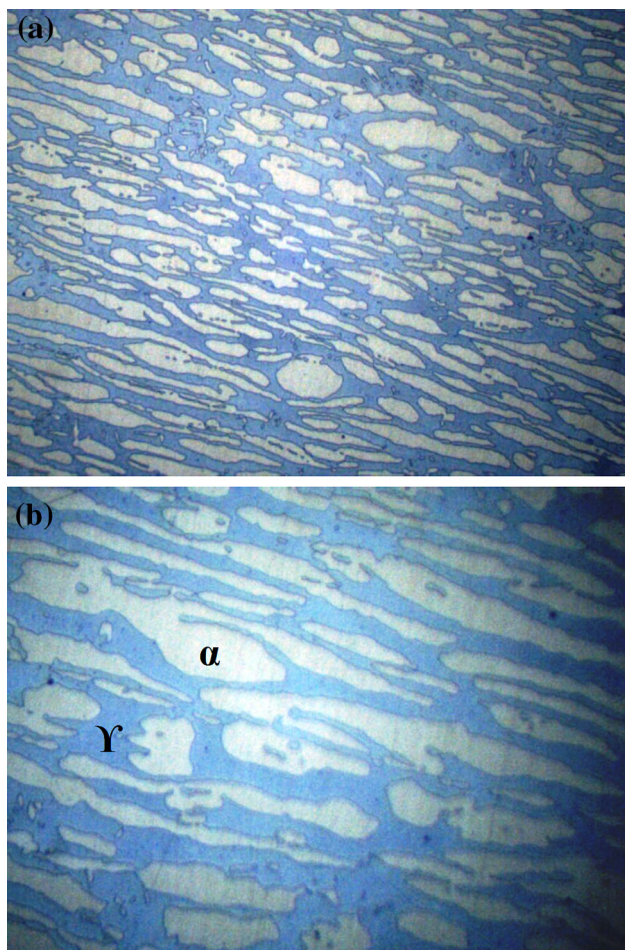

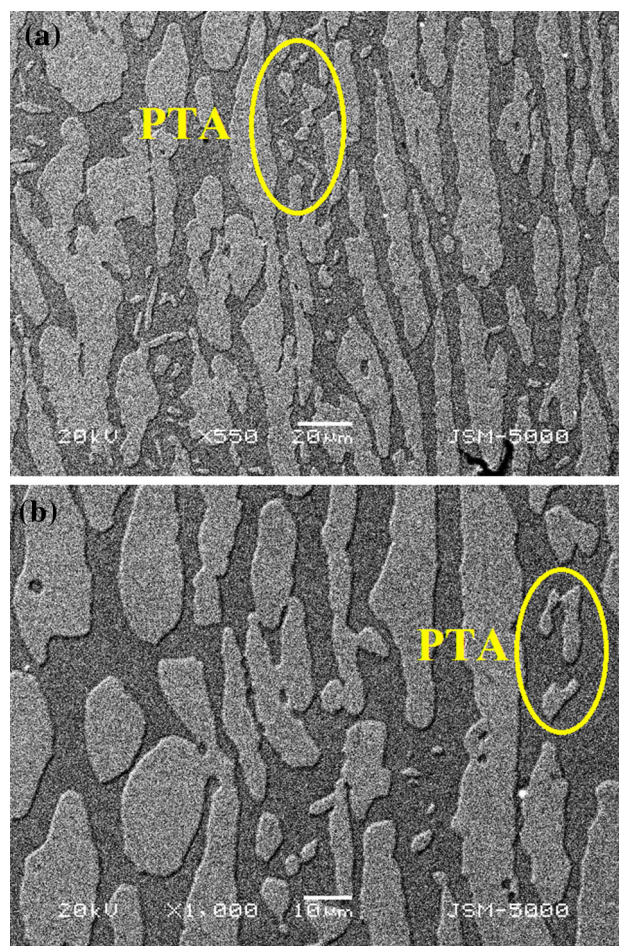**Fig. 1 a** Optical microstructure of HAZ at 200X. **b** Optical microstructure of HAZ at 400X

Fig. 2 a Scanning Electron Microscope (SEM) of HAZ at 20 μm. **b** Scanning Electron Microscope (SEM) of HAZ at 10 μm
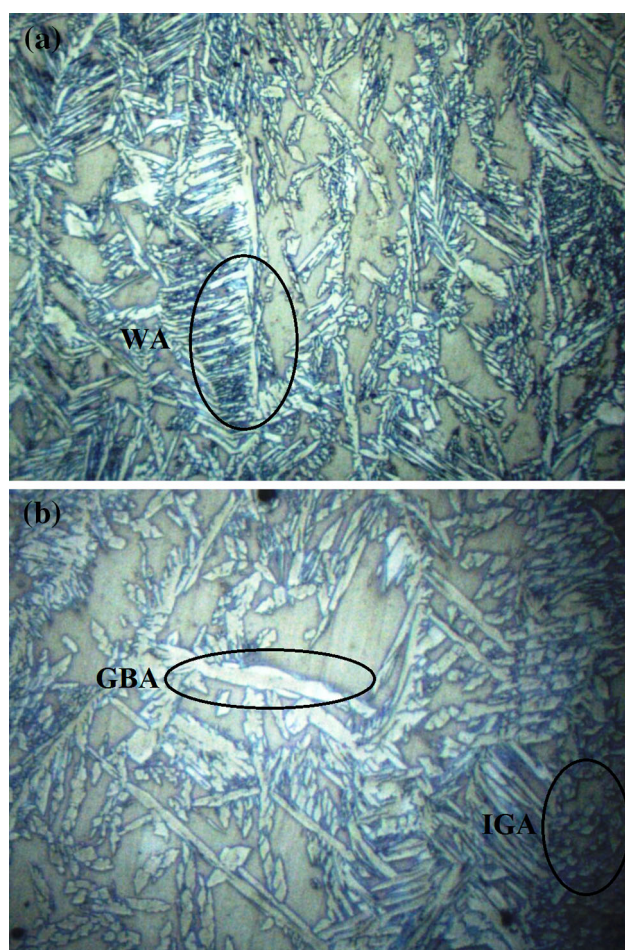
Fig. 3 a Optical microstructure of WZ at 200X. b Optical microstructure of WZ at 400X
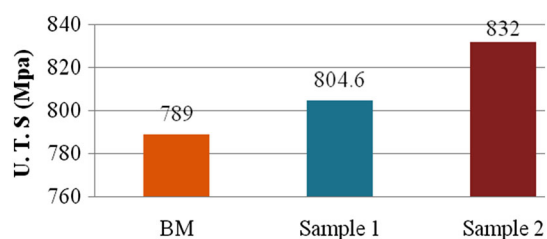

Fig. 4 Ultimate tensile strength comparison

2.4 Mechanical Properties

Universal testing machine FIE UTE-60 (maximum capacity 600kN) was used to carry out tensile tests. Two specimens were prepared for result consistency as per ASTM E8M-04 [36]. SEM and EDS were used to analyse mode of failure and chemical composition of the precipitates in the samples fractured by tensile test. Charpy impact tests using impact testing machine IT-30 were carried out at $-40°$ as per ASTM E-23:16b [37]. There were total six readings taken for impact test, three from WZ and three from HAZ, respectively. The vickers hardness tests were performed at HV 10 using brinell cum Vickers hardness tester BV-250 as per ASTM E 92:2017 [38]. There were five readings taken for each base metal and WZ as well as three readings taken for HAZ. The side bend test was performed having mandrel diameter of 40 mm at bend angle of 180° as per ASME Sec. IX-2017 [39].

3 Results and discussions

3.1 Non-Destructive Examination

Weld joint quality was investigated by X-ray radiography test (RT) at initial stage as per ASME Sec. V [40]. The RT was performed using ROLI-2 board of radiography and isotope technology (BRIT), BARC with the source of Iridium 192 having inspection range of 10 mm to 70 mm. Remote operated camera was used for RT and placed at a distance of 8 m from welded specimen. The RT result showcases the visible image quality indicators (IQI) identity of 7th wire from the required 9th wire. This shows no significant defect and the welded joint is accepted.

3.2 Ferrite Measurement

Quantitative morphology of ferrite measurement is observed as per ASTM E562-11 by image analyzer for BM, HAZ and WZ [41]. The results of ferrite measurement are given in Table 4. Average ferrite content in HAZ and WZ is higher than the minimum required limits ($\approx 30\%$)
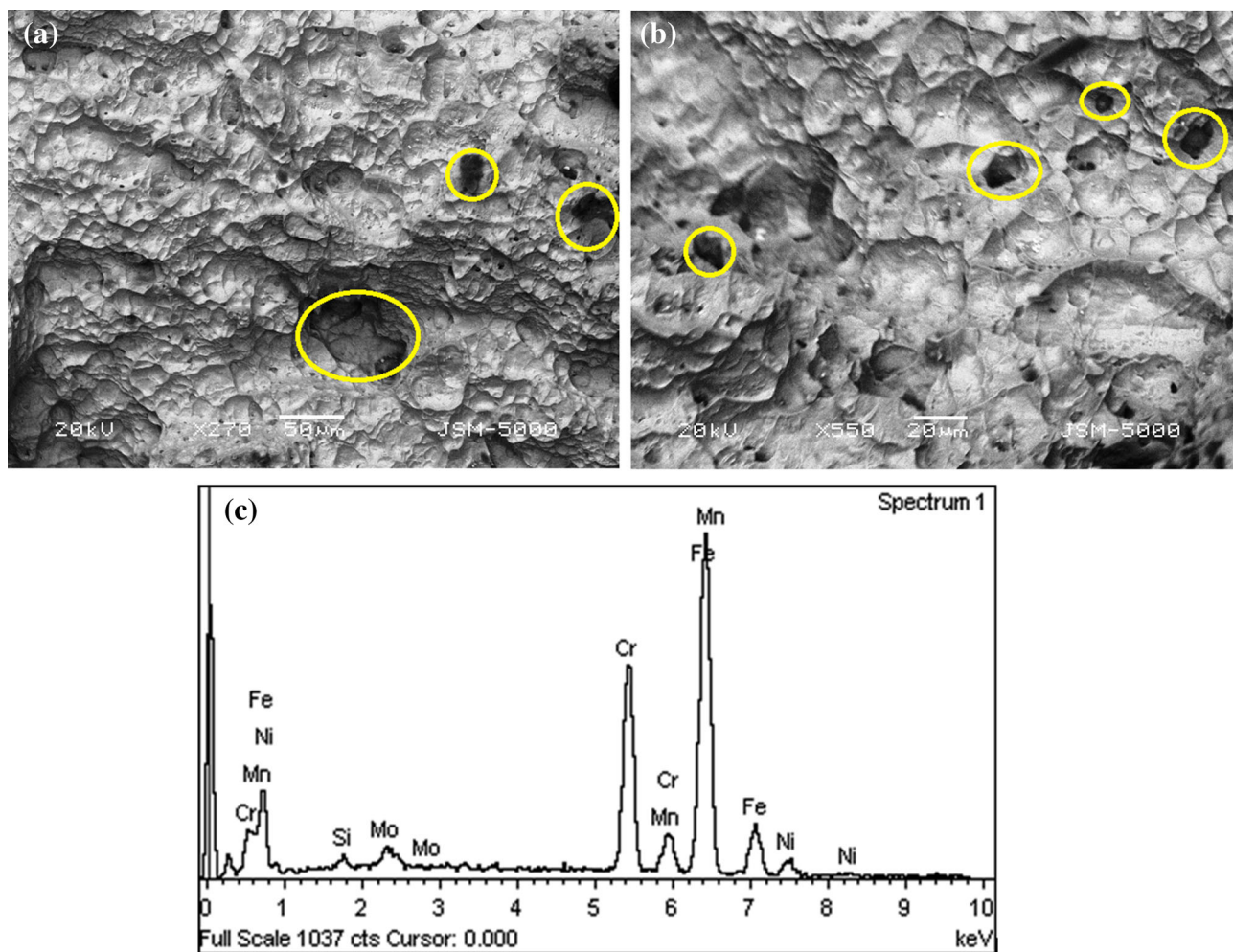
Table 5 Tensile test results

Sample	U.T.S. (MPa) 655 Min	Broken from	Fracture
1	804.6	Parent	Ductile
2	832.0	Parent	Ductile

Fig. 5 a Scanning electron microscope of tensile sample at failure. **b** Scanning electron microscope of tensile sample at failure. **c** Energy Dispersive Spectroscopy spectrum of the precipitates

Table 6 V notch Charpy impact test result

| Location	Obtained value	
	Size of specimen: 10 mm $\times$ 10 mm and test temperature: $-$ 40°C	
	Weld	HAZ
Energy absorbed (Joules) 1	78	106
Energy absorbed (Joules) 2	72	96
Energy absorbed (Joules) 3	80	106
Avg. values (Joules)	76.67	102.67

which results in better mechanical properties. Ferrite content decreases in HAZ and WZ due to low cooling rates to regain austenite from δ ferrite and difference between thermal cycles of two regions. Cooling rate is calculated based on temperature raised during welding (above 150 °C) and time taken to cool down up to150°C. So, it shows average cooling rate from 6.33 °C/sec to 1.19 °C/sec at low and high heat input, respectively.

3.3 Microstructure Investigation

Optical microscopy is performed to investigate intermetallic phases on WZ and HAZ as per ASTM A923. Initially samples were polished by using 80 and 120 grit papers. The electro etching solution was made by addition of 40gm reagent grade sodium hydroxide (NaOH) into 100gm of distilled water at 1–3 V for 50 s. Microstructures

Table 7 Vickers hardness test results

Location	Obtained value in HV-10	Average value in HV-10
WZ	253,251,254,253,255	253.2
HAZ (left of WM)	221,222,219	220.66
HAZ (right of WM)	220,222,221	220.83
BM (left of WM)	193,194,192,191,195	193
BM (right of WM)	190,193,194,191,192	192
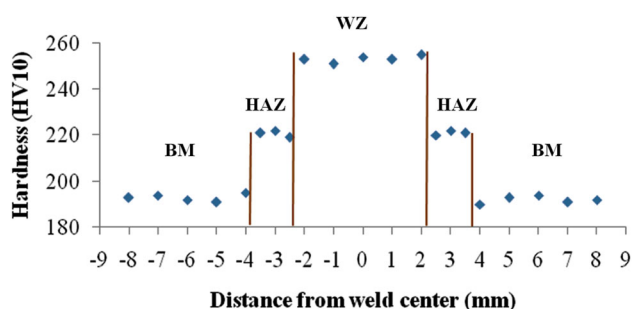
Fig. 6 Vickers hardness across the weld

were examined by using optical metallurgical microscope NIM1000x having range of 10X to 1000X. The optical microstructures of HAZ are depicted in Fig. 1a at 200X and in Fig. 1b at 400X.

Electro-etching has been used to reveal to differentiate different colored shade of austenite (α) and ferrite (ϒ). Figure 1b showcases light color for austenite and dark color for ferrite. The interphase boundaries are found to be smooth as shown in Fig. 1a which clearly indicates no significant effect of intermetallic or nitride phase in HAZ. Thus HAZ can be considered as an unaffected structure and is acceptable as per ASTM A923.

The scanning electron microscope (SEM) images of HAZ in Fig. 2a at 20 μm and in Fig. 2b at 10 μm show no significant effect of intermetallic phases. It also reveals that microstructure with partially transformed austenite (PTA) restricts the growth of grain. These results are in good agreement with Aman Gupta et.al. (2018) [1].

The optical microstructures of WZ are depicted in Fig. 3a at 200X and in Fig. 3b at 400X. Figure 3a illustrates fine waviness at interface boundaries which reveal that dendritic structure and widmanstatten austenite (WA) are present in the structure. Dendritic structure showcases

tree like structure of crystals and grow as molten metal solidifies after welding. Figure 3b illustrates intragranular austenite (IGA) and grain boundary austenite (GBA). Austenite at grain boundary starts to develop at grain boundary of δ ferrite and then formation of widmanstatten austenite occurs which propagates within the grains due to cooling. While intra granular austenite nucleates and grow within the δ ferrite grain. Figure 3b illustrates separated grain boundaries because of widmanstatten austenite which result in coarse structure.

3.4 Mechanical Properties

In this present investigation, tensile test, charpy impact test, microhardness vickers test and side bend test have been carried out to quantify mechanical properties of weldments. Two specimens have been tested for tensile test, and it showcase ultimate tensile strength (UTS) for both the welded specimens which are 804.6 MPa and 832 MPa. These are better than that of BM 789 MPa as shown in Fig. 4.

During tensile test, both weldment specimens show ductile fracture with specimens broken from the parent and detail of the test is given in Table 5.

The fractograph of tensile sample is shown by SEM images including EDS in Fig. 5. The fractured surface showcases presence of finer circular structure as in Fig. 5a as well as square precipitates in Fig. 5b develops during welding. Finer precipitates result in good tensile strength [1, 42]. Figure 5c shows complex metal oxide precipitates containing Fe, Cr, Ni, Mn, Mo and Si in major proportion. Figure 7 reveals that precipitation of metal oxides may be the reason of failure.

Table 8 Side bend test results

Mandrel diameter (mm)	Angle of bend	Result
40	180°	No defect

Fig. 7 Side bend test sample

The V-Notch Charpy impact test for the HAZ and WM specimens is given in Table 6. During test, it has been found that failure is ductile and HAZ have more capacity to absorb energy than WM. From the impact test, it has been observed that WM and HAZ specimens have average impact value of 76.67 J and 102.67 J, respectively, which are more than that of minimum requirement of 36 J for WM and 54 J for HAZ. Higher ferrite percentage is observed in HAZ compared to WM resulting in higher impact strength in HAZ and also the optical micrographs reveals that finer grain boundaries are found in HAZ.

The vickers hardness test results are shown in Table 7. It shows that WZ having higher average hardness of 253.2 HV10 than HAZ and BM. Figure 6 represents the vickers hardness across the weld which reveals that higher hardness in WZ is due to the formation of secondary austenite phase. This phase frequently has high molybdenum and chromium content because of multipass welding which leads to the growth of austenite phase [43–45].

The side bend test result of weldment is highlighted in Table 8, and the bend has been carried out for 180° using 40-mm-mandrel which reveals satisfactory result as shown in Fig. 7.

However, all the above results show good agreement with literature studied in this investigation, and its comparison is shown in Table 9.

3.5 . Conclusions

In this present work, mechanical properties and microstructures of DSS 2205 weldment are examined for thick section using shielded metal arc welding (SMAW) and E2209 electrode which conclude that:

1. In microstructure results, widmanstatten austenite (WA), intragranular austenite (IGA) and grain boundary austenite (GBA) were observed in WZ microstructure of the weldment. This type of microstructure was found because of grain growth of δ ferrite inside the grain and cooling rate during solidification of welding. Cooling rate depends on heat input during welding. In this investigation, heat input was maintained from 0.95 to 1.35 kJ/mm with cooling rate of 6.33–1.19 °C/sec at 150 °C interpass temperature. However, microscopic investigation also revealed that no intermetallic phase was observed in weldment.

2. For quantitative morphology of ferrite measurement, average ferrite content was observed to be 43.526%, 48.219% and 50.788% in WZ, HAZ and BM, respectively. Low ferrite content was observed in WZ due to Interpass temperature of 150 °C, which allowed weldment to regain austenite during cooling cycle.

3. Ultimate tensile strengths (UTS) were observed to be 804.6 MPa and 832 MPa with ductile failure. Higher value of UTS at weldment indicated presence of Cr, Mo, Ni, Mn and Si in major proportion which enhanced mechanical properties. Average impact strength was found to be 76.67 J and 102.62 J in WZ and HAZ, respectively. Higher impact strength was observed in HAZ because of higher ferrite content present in HAZ. Vickers hardness was observed to be higher 253.2 in WZ, and side bend test showed satisfactory results for the weldment.

4. However, this present investigation revealed that SMAW process produced satisfactory results for multi-pass welding of DSS thick plate with no significant defects. The results retrieved from experiments met the requirements of ASME/ASTM standards.

Table 9 Results Compared with literature

Output	Findings	Literature mapped
Microstructure	WA, GBA and IGA at WZ PTA at HAZ (no inetrmetallic phase observed)	[1, 4, 12, 16] and [42]
Ferrite content (Table 4)	BM > HAZ > WZ (far better than literature)	[1, 10, 11] and [42]
Mechanical Properties (Table 5, 6, 7 and 8)	Tensile, impact, vickers hardness and side bend test (meeting all the requirements of ASME/ASTM standards)	[1, 11, 12, 16] and [42]

References

[1] Gupta A, Kumar A, Baskaran T, Arya S B, and Khatirkar R K, *Transactions of the Indian Institute of Metals* 71 (2018) 1595.

[2] Lippold J C, and Kotecki D J, *Welding Metallurgy and Weldability of Stainless Steels*, Wiley Interscience, New Jersey (2005).

[3] Nilson J O, *Mater Sci Tech* 8 (1992) 685.

[4] Haghdadi N, Laleh M, Kosari A, Moaye, M H, Cizek P, Hodgson P D, and Beladi H, *Materials Letters* 238 (2019) 26

[5] Nomani J, Pramanik A, Hilditch T, and Littlefair G, *Wear* 304 (2013) 20.

[6] Ebrahimi N, Moayed M H, and Davoodi A, *Corrosion Science* 53 (2011) 1278.

[7] Mourad A I, Khourshid, A, and Sharef T, *Materials Science and Engineering: A* 549 (2012) 105.

[8] Sieurin H, and Sandstrom R, *Mater Sci A* 418 (2006) 250.

[9] Zhang Z, Wang Z, Jiang Y, Tan H, Han D, Guo Y, and Li J, *Corrosion Science* 62 (2012) 42.

[10] Zhang Z, Jing H, Xu L, Han Y, Zhao L, Lv X, and Zhang J, *Applied Surface Science* 435 (2018) 352.

[11] Migiakis K, and Papadimitriou G D, *Journal of Materials Science* 44 (2009) 6372.

[12] Muthupandi V, Srinivasan P B, Seshadri S K, and Sundaresan S, *Materials Science and Engineering: A* 358 (2003) 9.

[13] Kou S, *Welding Metallurgy*, Wiley Interscience, New Jersey (2003).

[14] Sieurin H, and Sandström, R, *Materials Science and Engineering: A* 444 (2007) 271.

[15] Llorca-Isern N, López-Luque H, López-Jiménez I, and Biezma M V, *Materials Characterization* 112 (2016) 20.

[16] Ramkumar K D, Mishra D, Raj B G, Vignesh M K, Thiruvengatam G, Sudharshan S P, and Rabel A M, *Materials & Design* 66 (2015) 356.

[17] Kim S T, Jang S H, Lee I S, and Park Y S, *Corrosion Science* 53 (2011) 1939.

[18] Chen T H, and Yang J R, *Materials Science and Engineering: A* 311 (2001) 28.

[19] Zanotto F, Grassi V, Merlin M, Balbo A, and Zucchi F, *Corrosion Science* 94 (2015) 38.

[20] Kim S T, Lee I S, Kim J S, Jang S H, Park Y S, Kim K T, and Kim Y S, *Corrosion science* 64 (2012) 164.

[21] Lopez N, Cid M, and Puiggali M, *Corrosion Science*, 41 (1999) 1615.

[22] Kwok C T, Lo K H, Chan W K, Cheng F T, and Man H C, *Corrosion science* 53 (2011) 1581.

[23] Takei T, Yabe M, and Wei F G, *Corrosion Science* 122 (2017) 80.

[24] Deng B, Jiang Y M, Gao J, and Li J, *Journal of Alloys and Compounds* 493 (2010) 461.

[25] Pohl M, Storz O, and Glogowski T, *Materials characterization* 58 (2007) 65.

[26] Tan, H, Jiang Y, Deng B, Sun T, Xu J, and Li J, *Materials Characterization* 60 (2009) 1049.

[27] Kashiwar A, Vennela N P, Kamath S L, and Khatirkar R K, *Materials Characterization* 74 (2012) 55.

[28] Hertzman S, Nilsson M, and Jargelius-Pettersson R (1994), *Proc. Duplex Stainless Steels1994 Glascow Scotland: Paper I* (1994).

[29] Schaeffler A L, *Met Prog* 56 (1949) 680.

[30] Delong W, Ostrom G, and Szumachowski E, *Weld J* 35 (1956) 526s.

[31] Kotecki D J, and Siewert T A, *Weld Res Suppl* (1992) 171s.

[32] ASTM E1086-14, *Standard Test Method for Analysis of Austenitic Stainless Steel by Spark Atomic Emission Spectrometry* (ASTM International, Philadelphia, 2014)

[33] ASME Boiler and Pressure Vessel code, Section V, *Nondestructive Examination*, American Society of Mechanical Engineers (2017)

[34] ASTM E3-95, *Standard Practice for Preparation of Metallographic Specimens*, ASTM, PA, USA (1995).

[35] ASTM A923-14, *Standard Test Methods for Detecting Detrimental Intermetallic Phase in Duplex Austenitic/Ferritic Stainless Steels,* ASTM International, West Conshohocken, PA, (2014)

[36] ASTM E8/E8M-08, *Standard Test Methods for Tension Testing of Metallic Materials*, ASTM, West Conshohocken, PA, (2009)

[37] ASTM E23-16b, *Standard Test Methods for Notched Bar Impact Testing of Metallic Materials*, ASTM International, West Conshohocken, PA, (2016)

[38] ASTM E92-17, *Standard test methods for vickers hardness and knoop hardness of metallic materials*. West Conshohocken, PA, (2017)

[39] ASME, Boiler and Pressure Vessel Code Section IX: *Qualification Standard for Welding and Brazing Procedures, Welders, Brazers, and Welding and Brazing Operators*, The American Society of Mechanical Engineers, 2017.

[40] ASTM G108-94, *Standard Test Method for Electrochemical Reactivation (EPR) for Detecting Sensitization of AISI Types 304 and 304L Stainless Steels*, ASTM Book of Standards, American Society for Testing of Metals, Philadephia PA (2015)

[41] ASTM E562-11, *Standard Test Method for Determining Volume Fraction by Systematic Manual Point Count* (ASTM International, West Conshohocken, PA, 2011).

[42] Dandekar T R, Gupta A, Kumar A, Khatirkar R K, and Vadavadagi B, *Materials Research Express* 5 (2018) 106506.

[43] Tseng C M, Liou H Y, and Tsai W T, *Materials Science and Engineering: A* 344 (2003) 190.

[44] Rawers J, and Grujicic M, *Materials Science and Engineering: A* 207 (1996) 188.

[45] Wu M, Liu F, Pu J, Anderson N E, Li L, and Liu D, *Journal of Materials Engineering and Performance* 26 (2017) 5341.